

Numerical Simulations of Solvent Effects on Optical Transmission Processes for Zinc Porphyrins

Masato Nakashima*, Landa Hoke**, Brian R. Kimball
Barry S. DeCristofano, and Paula Rosenof
Materials Science Team, U.S. Army Soldier Systems Center, Natick, MA 01760

Gregory J. Kowalski***
Department of Mechanical, Industrial, and Manufacturing Engineering,
Northeastern University, Boston, MA 02215

Desai Narayana Rao
School of Physics, University of Hyderabad, Hyderabad, India

D.V.G.L.N. Rao
Department of Physics, University of Massachusetts, Boston, MA 02125

ABSTRACT

The optical transmission processes for a nonlinear optical (NLO) material are influenced by the properties of its environment. NLO properties such as intersystem crossing rates may be altered by characteristics of the host such as polarity. The effects of the host material on the optical transmission of the NLO material is investigated using numerical laser beam propagation modeling (LBPM) techniques. Numerical simulations are reported for the optical transmission for zinc meso-tetra(p-methoxyphenyl)tetrabenzporphyrin (ZnTMPTBP) in liquids of differing polarity such as toluene, tetrahydrofuran (THF), dichloromethane (DCM), acetone, and pyridine. In addition to investigating the effect of the solvent on transmission, these calculations explore the effect on transmission of two different singlet lifetimes which have been reported in the literature. Transmission curves are calculated using separately determined parameters obtained from curve fitting using zscan data. Calculated results are compared with experimental data for all cases. Z-scans are also calculated for several cases and the results compared to experimental data. Numerical simulations provide a valuable tool to study the optical transmission behavior of NLO materials such as ZnTMPTBP.

Keywords: Nonlinear optical materials, Thermally stimulated nonlinear effects, Zinc porphyrins, Solvent effects, Laser beam propagation

1. INTRODUCTION

The environment of a zinc porphyrin affects the optical properties of this NLO material. Earlier work¹ examined this phenomenon using optical transmission curves and zscans. This current work is an application of laser beam propagation modeling (LBPM) methods to investigate the solvent effects on absorption of radiation by zinc porphyrins. For this current work zinc meso-tetra(p-methoxyphenyl)tetrabenzporphyrin (ZnTMPTBP) was investigated for five solvents: toluene, THF, DCM, acetone, and pyridine.

In order to perform the optical transmission calculations, values were required for the cross-sections and lifetimes for ZnTMPTBP in each solvent. To obtain these values nanosecond (ns) zscan data were collected with 6 ns (FWHM) pulses with a 1 mm pathlength and 80 mm focal length and this data was used as the basis for a Runge-Kutta fourth order (RK4)



least squares type analysis to predict the NLO parameters. Initial assumptions and therefore constraints to this curve fitting process were the values of the first and second singlet lifetimes as well as the values of the first and second triplet lifetimes. These were assumed to be the same for all solvents. Based on this information and the zscan data, values were predicted for the intersystem crossing rate and the cross-sections (ground, singlet, triplet) for different solvents. These independently obtained parameters were used as input for LBPM calculations of optical transmittances. The pulse width for the optical transmittance calculations was 10 ns (FWHM) with a 2 mm pathlength. The optics for these transmission simulations is $f/5$ and the wavelength of the laser is 532 nm. The focal length was 100 mm. The focal plane was placed at the back (beam exit) face of the sample.

Singlet lifetimes of different magnitudes have been reported for ZnTMPTBP^{2,3}. A least squares RK4 type analysis using an assumption of a singlet lifetime of 40 ps was reported previously¹. New least squares analyses were completed by one of us (DNR) based on the same ns zscan data as the 40 ps analysis but using an initial assumption of a 400 ps singlet lifetime for this current work. Cross-sections and lifetimes predicted using each of these two assumptions were used in two sets of calculations and comparisons are made with experimental data.

Most calculations for optical transmittances assumed a volumetric expansion coefficient of zero and did not include the thermal expansion effects and their associated refraction changes after laser irradiation on transmission processes. Although the expansion of the host due to laser heating was not included in most calculations, the effects of volumetric expansion due to laser beam heating on the predicted transmittances was included for selected cases.

In addition to calculations of optical transmission curves, the LBPM method was used to predict open aperture zscans in the ns and also the ps temporal regimes. For the ns zscans the NLO parameters from the RK4 method using the 400 ps singlet lifetime assumption were used as input to the code for the solvents toluene, THF, and DCM. The LBPM method was then used to calculate ns zscans and comparisons made between calculated and experimental zscans.

Picosecond (ps) zscan data were also collected as part of the original experimental work¹. The pulse width for these experiments was 35 ps (FWHM) with a pathlength of 2 mm. The focal length was 118 mm. The RK4 method was again used based on the two initial assumptions of a 40 ps or a 400 ps singlet lifetime. NLO parameters predicted from each of these two assumptions were used in the LBPM method to calculate ps zscans in toluene. Calculations were also completed for THF and DCM. Comparisons are made with experimental data.

The objectives of this work are to compare calculated and experimental transmittances for optical transmission data and to study the effect of the singlet lifetime on the predicted values of these transmittances. Objectives are also to compare the results of ns and ps zscan calculations with zscan data. The objectives are also to demonstrate for the zscan calculations a consistency that was not achieved for the experimental data by specifying the same peak intensity for the incident laser beam for different solvents. NLO material concentrations for the ns zscan calculations were not the same for all solvents in an attempt to follow actual experimental specifications. However, the code provides a method where all parameters such as these can be specified to be the same for all solvents thus facilitating comparisons between solvents on the transmission for materials such as ZnTMPTBP.

2. PROCEDURE

2.1 Nonlinear optical and thermal Code

The numerical simulation code for the laser beam propagation model, (LBPM), is described in Whalen⁴, 1999, Kowalski⁵, 1996 and Kowalski et al⁶, 1995, for the Fourier transport models. The code allows the user to select the appropriate thermal transport model and it is divided into preprocessor and simulation functions. The preprocessor function uses the problem inputs to calculate the nodal system parameters required for the solution. The simulation function is a transient, three dimensional, finite difference algorithm that determines the thermal response interaction with the optical problem. It is written in a Cartesian coordinate system. The code includes the internal reflections of the beam, which are caused by the spatial gradient of the index of refraction. The index of refraction gradient is related to the temperature variation using the Lorentz-Lorenz law and the thermodynamic equation of state. The reflection from the sample as well as the transmitted intensity and optical phase changes through the sample area and also the temperature profile within the sample area are calculated by the code.

The thermal response of the material is described by the differential energy balance on it.

$$\nabla \cdot q = (\rho c_p / k_t) \frac{\partial T}{\partial t} - q_{abs} / k_t \quad (1)$$

The Fourier heat transfer model is used as the thermal transport mechanism.

$$q = -k_t \nabla T \quad (2)$$

The investigated sample region is centered on the incident beam and includes only the affected region. A 5x5x3 nodal system was used for the optical transmission simulations. The node spacing for the x and y directions was 17.5 μm and for the z direction the node spacing was 1mm. The air system interface is treated as adiabatic because of the short time of the laser pulse.

The absorbed radiation per volume, q_{abs} , is determined from the electromagnetic wave model. In this algorithm the incident wavefront is divided into a set of rays that are perpendicular to the beam wavefront. This treatment of the electromagnetic wave is valid for thin material layers. A similar approach is used in the previous literature by others, (Sheik-Bahae⁷, 1990 and Chen and Tien⁸, 1993). The node system is defined so that each ray is incident onto one node. An individual ray is followed as it travels through the sample area to calculate the thermal heating it causes as well the optical phase change and reflection it undergoes. Each ray is traced through the system and its contribution to the energy absorbed in each node and the energy reflected from each nodal volume interface is evaluated. The electromagnetic wave is taken to propagate in the z direction. In this model the spatial dependence of the total electric field E and total magnetic field H must satisfy the following relationship within the mth node volume

$$\frac{dy}{dz} = Ay \quad (3a)$$

where

$$y = \begin{bmatrix} E_x \\ H_y \end{bmatrix} \quad \text{and} \quad A = \begin{bmatrix} 0 & jk\mu_m \\ jk\epsilon_m & 0 \end{bmatrix} \quad (3b)$$

$$k = 2\pi/\lambda \quad (3c)$$

The magnetic permeability, μ_m , is assumed to be constant. The intensity and temperature variation of the complex dielectric coefficient is determined by relating it to the index of refraction.

Equations 3 are reformulated to obtain the radiative transport equation, RTE, which describes the absorption of the intensity within the node volume. The RTE is used to calculate the energy absorbed within the node volume, q_{abs} .

$$q_{abs} = \alpha_m (1 - R_m) I_{m-1} \exp(-((t - t_{pf})/tp)^2) (1 - \exp(-\alpha_m \Delta z_m)) \quad (4)$$

The nodal reflectance is determined from the electromagnetic wave model described by Eqs. 3.

The preceding equations are numerically solved by applying a spatial and temporal finite difference method. The temporal finite difference solution uses a modified Euler integration technique. The modified Euler integration technique is a predictor-corrector method that enables the code to include the nonlinear aspects of the problem.

The energy level diagram used in this investigation for the NLO material is schematically shown in Fig. 1; where, the N_i 's are the populations for each level, the σ_i 's are the one photon cross-sections, β is the two photon absorption cross-section, the k_i 's are the rate constants, and k_{13} is k_{ISC} (where ISC is intersystem crossing from the lowest excited singlet to the lowest triplet).

The absorption coefficient α is given by eqn. (5)

$$\alpha = \sigma_0 N_0 + \sigma_1 N_1 + \sigma_2 N_2 + \beta I \quad (5)$$

The transient population density of the ground state and excited levels are determined using a five-level population model.

$$\frac{dN_0}{dt} = -\frac{\sigma_0 I N_0}{h \nu} + \frac{N_1}{\tau_1} + \frac{N_3}{\tau_4} - \frac{\beta I^2}{2h\nu} \quad (6)$$

$$\frac{dN_1}{dt} = +\frac{\sigma_0 I N_0}{h \nu} - \frac{\sigma_1 I N_1}{h \nu} - \frac{N_1}{\tau_1} - \frac{N_1}{\tau_{ISC}} + \frac{N_2}{\tau_2} \quad (7)$$

$$\frac{dN_2}{dt} = -\frac{\sigma_1 I N_1}{h \nu} - \frac{N_2}{\tau_2} + \frac{\beta I^2}{2h\nu} \quad (8)$$

$$\frac{dN_3}{dt} = -\frac{\sigma_2 I N_3}{h \nu} + \frac{N_1}{\tau_{ISC}} - \frac{N_3}{\tau_4} - \frac{N_4}{\tau_3} \quad (9)$$

$$\frac{dN_4}{dt} = -\frac{\sigma_2 I N_3}{h \nu} + \frac{N_4}{\tau_3} \quad (10)$$

where h is Planck's constant and ν is the frequency of the incident laser radiation.

The system of differential equations for the populations, N_0 , N_1 , N_2 , N_3 and N_4 of the five level model is solved using the same modified Euler predictor-corrector technique used in the thermal model. The transmitted energy through the sample is calculated by spatially and temporally numerically integrating the ray intensity at the exit of the sample.

2.2 Code inputs

Code input values for the solvent properties are provided in Section 2.2.1 and the NLO property values are provided in Section 2.2.2.

2.2.1 Solvent input properties

The solvent parameters used in the calculations are provided in Table 1. The effects of volumetric expansion were neglected for most calculations. A nonzero value of the volumetric expansion coefficient was used in selected calculations.

2.2.2 NLO properties

2.2.2.1 ns Calculations (optical transmission curves and zscans)

NLO input properties for ns calculations are provided in Table 2. Two categories of ns calculations were conducted. The first is optical transmission calculations. For these calculations a value for the ground state cross-section was calculated from spectroscopically measured extinction coefficients. These values along with the corresponding ground state extinction coefficients are provided in the table. This ground state cross-section is the most accurate value we have for ZnTMPTBP in each solvent.

The second category of calculation is a ns zscan. For the zscan calculations all NLO properties used for code inputs are from the RK4 curve fitting including the ground state cross-section. In the previous work¹, the ns NLO parameters were obtained from curve fitting using an assumption of a 40 ps singlet lifetime for ZnTMPTBP. New curve fitting was completed for this current work using an assumption of 400 ps for the singlet lifetime. Predicted NLO properties using each of these assumptions are shown in Table 2. Calculations are reported here for each of these two assumptions for the singlet lifetime.

2.2.2.2 ps NLO properties

The NLO parameters used for the ps zscan calculations are provided in Table 3.

3. RESULTS AND DISCUSSION

The results for the optical transmittance curves are presented in Section 3.1. Section 3.2 examines the inclusion of thermal effects. Sections 3.3 and 3.4 provide the results for ns and ps zscans. Section 3.5 provides a discussion of factors which affect the calculated results.

3.1 Optical transmission curves for volumetric expansion coefficient of zero

Comparisons of calculated and experimental results are shown in Fig. 2.

Table 4 shows the energies where the transmittances are approximately one-half the linear transmittances for toluene, THF, DCM and acetone for the 400 ps singlet lifetime assumption. The 400 ps assumption was chosen because this was closer to the experimental data than the 40 ps lifetime assumption for the optical transmission results. Table 4 thus provides a comparison of the effects of the different solvents on the effectiveness of ZnTMPTBP to attenuate the incident laser radiation. Both calculated and experimental results suggest that toluene is one of the better hosts of the four solvents compared for facilitating laser attenuation for ZnTMPTBP.

In the sections below results are discussed for the optical transmittance curves in each of the five solvents. Table 5 provides quantum efficiencies for each of the solvents based on code input parameters along with the ratios of the triplet to ground state cross-sections used for the calculations.

3.1.1 Toluene

Figure 2 (a) shows a comparison of calculated and experimental results for ZnTMPTBP in toluene for optical transmission calculations. The calculated results show correspondingly higher transmittances than the experimental data. A comparison of the two sets of calculated results shows that the 400 ps singlet has lower predicted transmittances than the 40 ps singlet results. These results are expected based on quantum efficiencies and ratios of the triplet cross-sections to the ground state cross-sections. The quantum efficiency for the 400 ps case is 44.4% with a ratio of 2.39. The quantum efficiency of the 40 ps case is 7.41% with a ratio of 2.23. Therefore, the quantum efficiency is about six times greater for the 400 ps case. Consequently, for the 400 ps case, many more NLO molecules are decaying to the first excited triplet than back down to the ground state. Since the triplet cross-section is more than two times greater than the ground state cross-section for each case, the transmittance is expected to be smaller for the 400 ps case as shown in Figure 2 (a).

3.1.2 THF

As in the case of toluene, the solvent THF shows greater transmittances for the 40 ps case than for the 400 ps case. This is shown in Figure 2 (b). Again, the quantum efficiency is a factor of 8.5 times greater (16.67% vs 1.96%) for the 400 ps case than for the 40 ps case and the ratio of the triplet cross-section to the ground state cross-section is about 2 for each case. Therefore, these results would be expected.

3.1.3 DCM

Figure 2 (c) shows that for the solvent DCM, the 40 ps and 400 ps calculated transmittances are about the same. A comparison of the quantum efficiencies show that the 400 ps case is 88.89% while the 40 ps case is 44.44%. This is only a factor of about 2 (versus 6 for toluene and 8.5 for THF). In addition the ratio of the triplet to the ground state cross-section is 1.31 which is much less than that for either toluene or THF. Therefore, not as much discrepancy between the predicted transmittances would be expected for the 40 ps and the 400 ps cases.

3.1.4 Acetone

Figure 2 (d) shows that the 40 ps case has greater predicted transmittances than the 400 ps case for acetone. The quantum efficiency of the 400 ps case is 7.41% versus 2.60% for the 40 ps case. Hence, the 400 ps case is only 2.85 times greater with respect to quantum efficiency. However, for the solvent acetone, the ratio of the triplet cross-section to the ground state cross-section is larger than for any of the other solvents evaluated here. Consequently, even a smaller increase in quantum efficiency for the 400 ps case would result in correspondingly less transmittance. In addition, the ratio of the

triplet to the ground state cross-sections is greater for the 400 ps case than for the 40 ps case. This will further decrease the expected transmittances for the 400 ps case. Therefore, the calculated results shown in Figure 2 (d) are reasonable.

3.1.5 Pyridine

Figure 2 (e) shows the results for pyridine. There were no new NLO parameters available for the 400 ps case. Therefore, only the 40 ps case can be examined. As opposed to the other solvents, for the solvent pyridine, the triplet cross-section was predicted to be smaller than the ground state cross-section with a ratio of 0.59.

Pyridine reacts reversibly with zinc porphyrins forming 1:1 complexes. In neat pyridine a porphyrin exists predominantly as a complex. In our case, however, in the analysis of zscan data, the complexation has not been taken into consideration in deriving various parameters. This neglect of the reactions involving the complexation might be the cause of the increase in the calculated transmission values with an increase in the input energy before the decrease takes place.

3.2 Optical transmission calculations with thermal effects included

The predicted transmittance values are less when thermal is included than when it is not included. For example, at an input energy of 10 μJ , toluene has a predicted transmittance of 0.1853 when thermal effects are included and 0.2134 when thermal is not included (400 ps singlet assumption). Similarly for THF at this same input energy, without thermal the transmittance is predicted to be 0.1422 and with the inclusion of thermal the transmittance is calculated to be 0.1626 (400 ps singlet). This is explained by the beam spreading resulting from sample heating and volume expansion. The less intense beam has less limiting due to less excited state absorption. Even though toluene is predicted to provide a better limiting environment in the low to mid energy ranges, at this relatively high input energy, THF is predicted to provide a better limiting environment for ZnTMPTBP. It should be noted that the concentration of the THF solution was approximately one-half that of the toluene solution. It would be of interest to make a similar comparison for solutions of equivalent concentrations.

Although no temperatures are reported here, the code has the capability to predict temperatures and could be used to compare the temperature rise for Zn TMPTBP in different solvents. This is of interest because the code can account for both excited state absorption by the NLO molecule as well as solvent thermal properties such as density, thermal conductivity, and specific heat. The temperature rise in the host due to laser heating is a function of all of these parameters.

3.3 ns zscans

Figs. 3(a), 3(b), and 3(c) show results for ns zscans for toluene, THF, and DCM. An example RK4 curve fit for toluene is shown in Fig. 3(a). The NLO parameters used for input to the LBPM calculations were based on these types of curve fits to the data.

Although calculated results for the LBPM method and the experimental results are shown on the same plots, there is not a direct correspondence. Concentrations as well as peak intensities for the laser beam were not the same for the calculated and experimental zscans. The peak intensity for the laser beam for both the LBPM calculations and the experimental data are shown on each plot for comparison. The differences in concentrations and peak intensities is suggested in differences between the calculated results and the experimental data for the $z = 0.0$ point for toluene. This also applies to THF where the experimental peak intensity is approximately one-half the value for the LBPM calculations. At the $z = 0.0$ point for THF, the transmittance is much lower for the calculated than the experimental results suggesting more attenuation due to the higher beam intensity.

In addition, there was not an exact correspondence for determining the Raleigh length for the LBPM calculations and for the RK4 method. The Raleigh length affects the NLO properties obtained from the curve fitting. Differences in Raleigh lengths would cause differences in intensities between the two methods and could give a different shape zscan curve as seen for the DCM case.

Considering these factors, the calculated results are in good general agreement with the experimental data.

3.4 ps zscans

Figs. 3(d), 3(e), and 3(f) show results for ps zscans for toluene, THF, and DCM. Again, for the same reasons provided in Section 3.3 above, a direct correspondence between calculated and experimental results is not expected. For the case of toluene, a comparison is included for a zscan predicted using the 40 ps singlet lifetime assumption with a zscan predicted using the 400 ps lifetime assumption. At the $z = 0.0$ position of the sample, the 400 ps case has a lower transmittance in agreement with results obtained for optical transmittance calculations in Section 3.1.

3.5 Considerations of factors which affect the results

Both the LBPM calculations and the RK4 curve fitting assumed a Gaussian spatial shape for the laser beam. The actual experimental beam shape is not a pure Gaussian. In addition, another consideration for the laser beam intensity values was that there was not an exact correlation between the calculation of the Raleigh length for the LBPM calculations and the RK4 curve fitting procedure.

While the LBPM calculations did include rises in temperature due to laser irradiation, most of these calculations did not include the consequent sample expansion and volume increase associated with the temperature rise. For the RK4 curve fitting calculations, temperature increases were not included in the five level model equations used as the basis for predicting the NLO input parameters.

We would expect the values of the ground state cross-sections to be the same for the ns and the ps cases and there were some differences. The differences in the ground state absorption cross-sections between the two sets of zscans are due to the instability of the material. We are testing improvements in the material handling.

4. CONCLUSIONS

NLO properties were extracted from ns zscan data and used as input to LBPM calculations to predict optical transmission curves. In comparing the experimental data and the calculated values using the properties extracted from the zscans, the latter consistently gave higher values for transmittances. Although the τ_{10} value of 400 ps puts the calculated values better in line with the experimental curves, the discrepancies did not warrant close comparison of parameters among the solvents. We are planning to test improvements for techniques to obtain NLO properties for inputs to LBPM calculations that will provide predicted transmittances in closer agreement with experimental optical transmission data.

5. REFERENCES

1. Kimball, Brian R., Nakashima, M., DeCristofano, Barry S., Srinivas, N.K.M. Naga, Premkiran, P., Rao, D. Narayana, Panchangam, Appaji, and Rao, D.V.G.L.N., "Solvent Effect on Optical Limiting of Zinc Tetrabenzoporphyrin Compounds, SPIE Proceedings, vol. 4106, pp. 264-271, 2000.
2. Rao, D. Narayana, Rao, S. Venugopal, Aranda, F.J., Rao, D.V.G.L.N., Nakashima, M., and Akkara, J.A., "Ultrafast Relaxation Times of Metaloporphyrins by Time-resolved Degenerate Four-wave Mixing with Incoherent Light" J. Opt. Soc. Am. B/14, (10), pp. 2710-2715, 1997.
3. Said, A.A., Dogariu, A., Xia, T., Hagan, D.J., and Van Stryland, E.W., "Nonlinear Optical Characterization of Zinc Tetra(p-methoxyphenyl)tetrabenzporphyrin", CLEO, Baltimore, 1995 The value of the lifetime was taken to be 400 ps for this current work, that is a value on the shorter end of the estimation in this reference in expectation of shorter average lifetimes among various solvents.
4. Whalen, R. A., "Numerical Modeling of Microscale Heat Transfer Effects in Thermally Stimulated Nonlinear Optical Materials," Ph.D. Thesis, Northeastern University, Boston, MA, 1999.
5. Kowalski, G.J., "Numerical Simulation of Transient Thermorefectance of Thin Films in the Picosecond Regime," High Heat Flux Engineering III, SPIE Vol-2855, pp 138-146, 1996.
6. Kowalski, G. J., Wahl, E.H. and Roach, J.F., "Numerical Simulation of Thermal Effects in Nonlinear Optical Materials," Materials for Optical Limiting, MRS Volume 374, Nov. 1995.
7. Sheik-Bahae, M., Said, A., Wei, T., Hagan, D. and Van Stryland, E., "Sensitive Measurements of Optical Nonlinearities Using a Single Beam," IEEE J. of Quantum Electronics, Vol. 26, No. 4, pp. 760-769, 1990.
8. Chen, G. and Tien, C.L., "Internal Reflection Effects on Transient Photothermal Reflectance," J. Appl. Phys., 73, pp. 3461-3466, 1993.

TABLE 1: Solvent properties

	TOLUENE	THF	DCM	ACETONE	PYRIDINE
ρ (Kg/m ³)	981.9	889.	1330.	791.	978.
C (J/Kg °K)	1698.	1720.	1190.	2174.	1676.
k (W/m °K)	0.131	0.120	0.122	0.161	0.165
n_{d20}	1.497	1.407	1.424	1.359	1.510
β (°K ⁻¹)	9.70E-4	1.00E-3	1.13E-3	1.36E-3	9.00E-4

TABLE 2: NLO properties for ns calculation

	TOLUENE	THF	DCM	ACETONE	PYRIDINE
ϵ (liter/mole/cm)	4100	5600	5400	3800	4200
σ_0 (m ² /molecule) ¹	1.57E-21	2.14E-21	2.06E-21	1.45E-21	1.61E-21
σ_0 (m ² /molecule) ²	2.33E-21	1.17E-21	1.61E-21	1.91E-21	1.91E-21
N_0 (molecules/m ³) ¹	2.618E23	3.145E23	1.777E23	2.9852E23	2.7009E23
N_0 (molecules/m ³) ²	3.524E23	1.151E24	4.559E23	4.542E23	4.542E23
τ_{21} (k ₂₁)	E-13 (E13)				
τ_{43} (k ₄₃)	E-13 (E13)				
τ_{30} (k ₃₀)	2E-4 (5E3)				
σ_1 (m ² /molecule)	5.5E-21	3.0E-21	5.1E-21	3.0E-21	2.1E-21
40 ps assumptio					
τ_{10} (k ₁₀)	40E-12 (2.5E10)				
τ_{ISC} (k ₁₃)	5E-10 (2E9)	2E-9 (5E8)	5E-11 (2E10)	1.5E-9 (6.67E8)	5E-11 (2E10)
σ_2 (m ² /molecule)	3.5E-21	4.0E-21	2.7E-21	3.7E-21	0.9E-21
β (m/W)	1.5E-10	0.4E-10	1.6E-10	0.8E-10	1.5E-10
400 ps					
τ_{10} (k ₁₀)	400E-12 (2.5E9)	400E-12 (2.5E9)	400E-12 (2.5E9)	400E-12 (2.5E9)	
τ_{ISC} (k ₁₃)	5E-10 (2E9)	2E-9 (5E8)	5E-11 (2E10)	5E-9 (2E8)	
σ_2 (m ² /molecule)	3.75E-21	4.0E-21	2.7E-21	4.25E-21	
β (m/W)	1.5E-10	0.4E-10	1.6E-10	0.8E-10	

1. Value used for optical transmission calculations 2. Value used for ns zscan calculations

TABLE 3: NLO properties for ps calculation

	TOLUENE	THF	DCM	ACETONE	PYRIDINE
σ_0 (m ² /molecule)	6.76E-22	6.39E-22	9.0E-22	9.32E-22	6.677E-22
N_0 (molecules/m ³)	6.072E23	1.054E24	4.078E23	4.654E23	6.496E23
τ_{21} (k ₂₁)	E-13 (E13)	E-13 (E13)	E-13 (E13)	E-13 (E13)	E-13 (E13)
τ_{30} (k ₃₀)	2E-4 (5E3)	2E-4 (5E3)	2E-4 (5E3)	2E-4 (5E3)	2E-4 (5E3)
σ_1 (m ² /molecule)	5.3E-21	3.25E-21	5.3E-21	3.0E-21	5.3E-21
σ_2 (m ² /molecule)	0.0E-21	0.00E-21	0.0E-21	0.0E-21	0.0E-21
40 ps assumptio					
τ_{10} (k ₁₀)	40E-12 (2.5E10)	40E-12 (2.5E10)	40E-12 (2.5E10)	40E-12 (2.5E10)	40E-12 (2.5E10)
τ_{ISC} (k ₁₃)	2E-9 (5E8)	2E-9 (5E8)	2E-9(5E8)	2E-9(5E8)	2E-9 (5E8)
β (m/W)	2.67E-10	2.67E-10	2.67E-10	2.67E-10	2.67E-10
400 ps					
τ_{10} (k ₁₀)	400E-12(2.5E9)		400E-12 (2.5E9)	400E-12 (2.5E9)	
τ_{ISC} (k ₁₃)	2E-9 (5E8)		2E-9(5E8)	1.5E-9 (6.667E8)	
β (m/W)	2.85E-10		2.75E-10	2.5E-10	

Note: No values were available for τ_{43} (k₄₃) for the ps case.

TABLE 4: Comparisons of transmission attenuations showing $\frac{1}{2} T_L$ experimental energy

	Calculated (400 ps Singlet Lifetime)	Experiment
Toluene	5.2 μ J	0.5 μ J
THF	15.3	1.1
DCM	84.6	0.4
Acetone	13.9	2.3

TABLE 5: Quantum efficiencies

	40 ps Singlet Lifetime		400 ps Singlet Lifetime	
	Ratio of σ_2 to σ_0	Quantum Efficiency	Ratio of σ_2 to σ_0	Quantum Efficiency
Toluene	2.23	7.41%	2.39	44.4%
THF	1.87	1.96	1.87	16.67
DCM	1.31	44.44	1.31	88.89
Acetone*	2.55	2.60	2.93	7.41
Pyridine	0.56	4.44		

* Note that tau(isc) is different for 40 ps vs 400 ps acetone

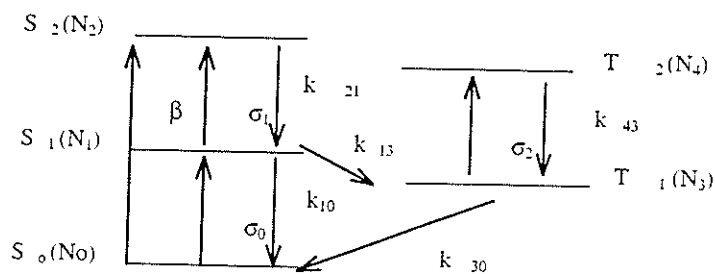
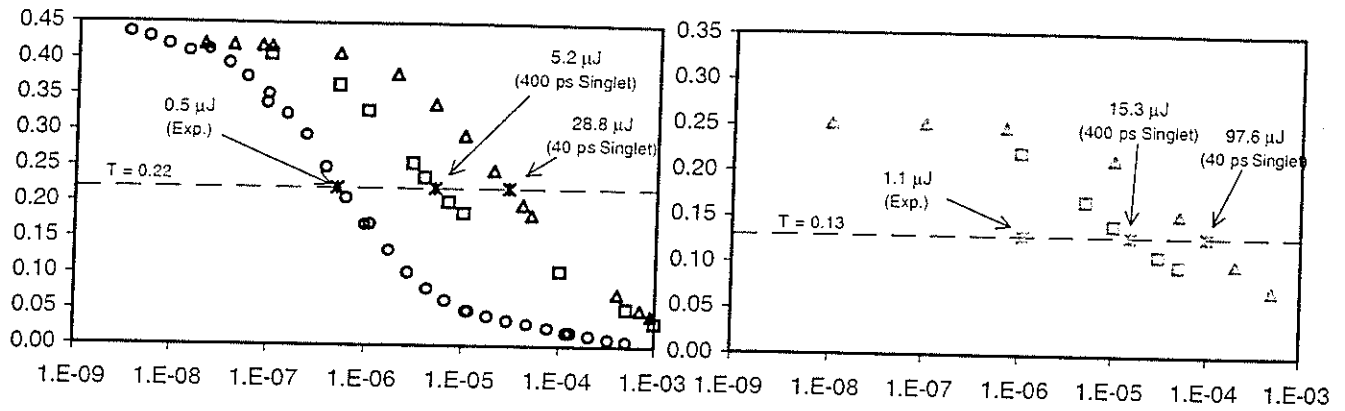


Fig. 1: Five level energy diagram

o Experiment Δ 40 ps Singlet Lifetime \square 400 ps Singlet Lifetime --- $\frac{1}{2} T_L$ (Exp.)

(a) Solvent: Toluene

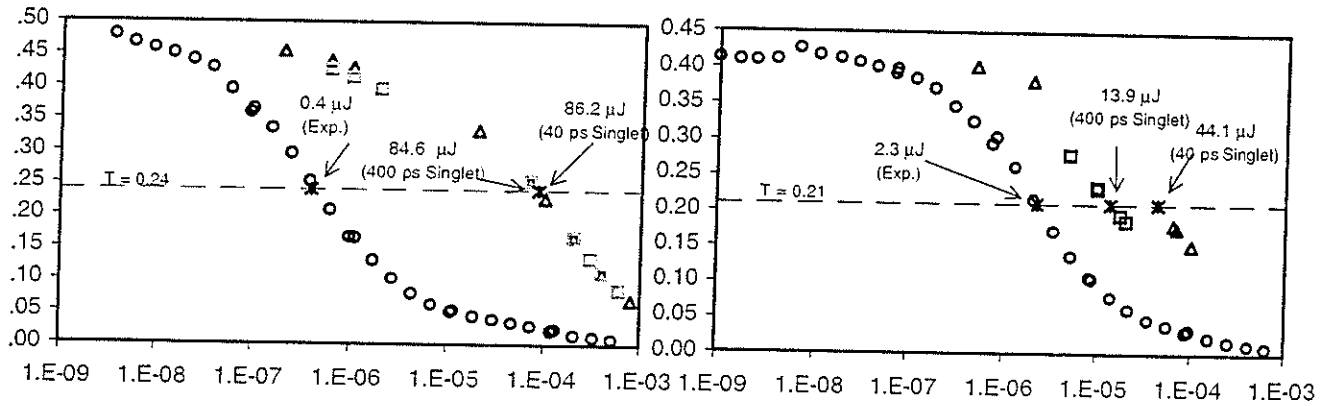
(b) Solvent: THF



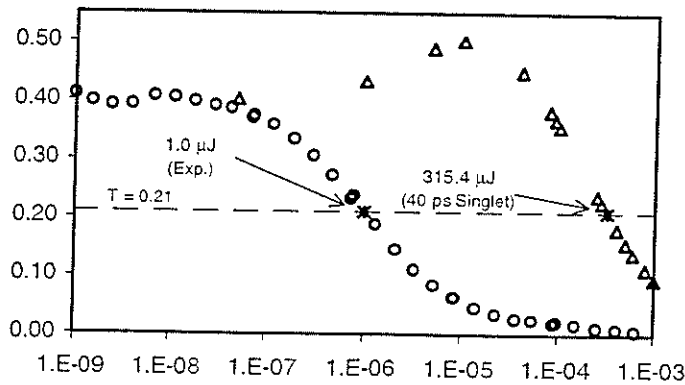
(c) Solvent: DCM

(d) Solvent: Acetone

T
R
A
N
S
M
I
T
T
A
N
C
E
S



(e) Solvent: Pyridine



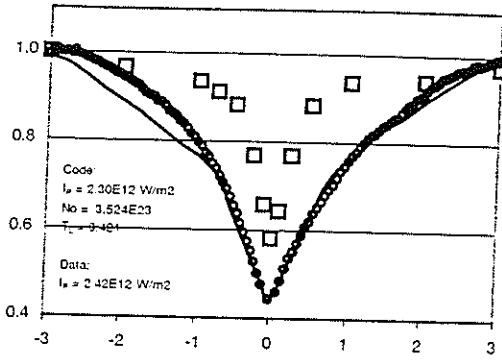
Sample Input Energy (Joules)

Fig. 2: Optical Transmittance Curves for Various Solvents: (a) Toluene, (b) THF, (c) DCM, (d) Acetone, and (e) Pyridine for Nanosecond Pulses

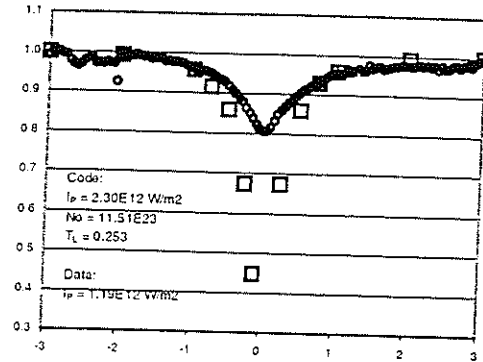
o Experiment Δ 40 ps Singlet Lifetime \square 400 ps Singlet Lifetime

TRANSMITTANCES

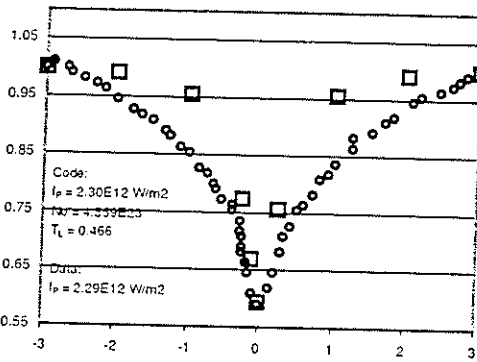
(a) Toluene (ns pulses)



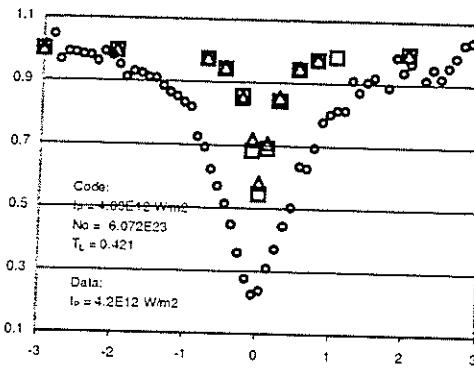
(b) THF (ns pulses)



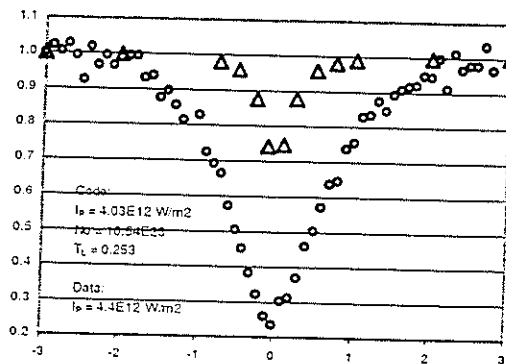
(c) DCM (ns pulses)



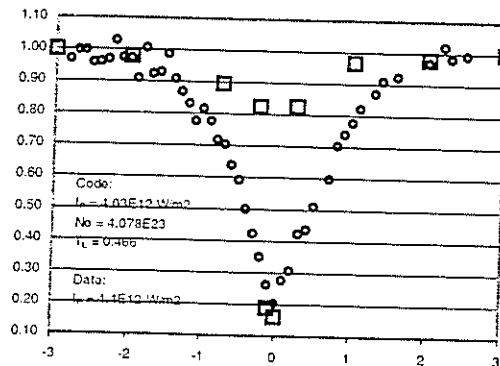
(d) Toluene (ps pulses)



(e) THF (ps pulses)



(f) DCM (ps pulses)



Sample Z Position (cm)

Fig. 3: Zscans: (a) Toluene (ns pulses), (b) THF (ns pulses), (c) DCM (ns pulses), (d) Toluene (ps pulses), (e) THF (ps pulses), and (f) DCM (ps pulses)